JOURNAL OF SYNCHROTRON RADIATION

ISSN 1600-5775

Received 25 April 2016
Accepted 10 February 2017

Edited by D. A. Reis, SLAC National Accelerator Laboratory, USA

Keywords: radiolysis; X-ray; synthesis; cupric oxide.

Caltrop particles synthesized by photochemical reaction induced by X-ray radiolysis

Akinobu Yamaguchi,[a]* Takao Fukuoka,[a] Iukuo Okada,[b] Mari Ishihara,[c] Ikuya Sakurai[b] and Yuichi Utsumi[a]

[a]Laboratory of Advanced Science and Technology for Industry, University of Hyogo, 3-1-2 Koto, Kamigori, Ako-gun, Hyogo 678-1205, Japan, [b]Synchrotoron Radiation Research Center, Nagoya University, Furo-cho, Chikusa-ku, Nagoya, Aichi 464-8603, Japan, and [c]Hyogo Prefectural Institute of Technology, 3-1-12 Yukihira, Suma, Kobe 654-0037, Japan. *Correspondence e-mail: yamaguti@lasti.u-hyogo.ac.jp

X-ray radiolysis of a $Cu(CH_3COO)_2$ solution was observed to produce caltrop-shaped particles of cupric oxide (CuO, Cu_2O), which were characterized using high-resolution scanning electron microscopy and micro-Raman spectrometry. X-ray irradiation from a synchrotron source drove the room-temperature synthesis of submicrometer- and micrometer-scale cupric oxide caltrop particles from an aqueous $Cu(CH_3COO)_2$ solution spiked with ethanol. The size of the caltrop particles depended on the ratio of ethanol in the stock solution and the surface of the substrate. The results indicated that there were several synthetic routes to obtain caltrop particles, each associated with electron donation. The technique of X-ray irradiation enables the rapid synthesis of caltrop cupric oxide particles compared with conventional synthetic methods.

1. Introduction

The synthesis of various metallic nanoparticles (NPs) has attracted considerable attention owing to the potential applications of NPs in various fields such as catalysis, medicine, electronics and optical-device engineering; interest has also been growing in the fundamental physics and chemistry of NPs (Kreibig & Vollmer, 1995; Le Ru & Etchegoin, 2009; Lu *et al.*, 2009; Cushing *et al.*, 2004). Recently, metallic NPs have been synthesized *via* numerous methods such as sonochemical reaction (Gedanken, 2004; Nagata *et al.*, 1992; Yeung *et al.*, 1993; Wagner & Köhler, 2005; Wagner *et al.*, 2004; Suslick *et al.*, 1991; Tu & Liu, 2000; Yamamoto *et al.*, 2004; Okitsu *et al.*, 2001), chemical aqueous reduction of metal ions (Frens, 1972, Frens, 1973), microwave-assisted synthesis (Athawale *et al.*, 2005; Tsuji *et al.*, 2005) and UV-visible light or laser-induced photochemical reaction (Takami *et al.*, 1999; Hashimoto *et al.*, 2011; Mafuné *et al.*, 2003; Bae *et al.*, 2002; Akamatsu *et al.*, 2004). In these studies, the presence of polyol and oxygen (Fievet *et al.*, 1989; Figlarz *et al.*, 1985; Kurihara *et al.*, 1995; Wiley *et al.*, 2004; Kvítek *et al.*, 2008; Hara *et al.*, 2015) plays a significant important role in synthesis and growth of nanoparticles. γ-ray and X-ray radiolysis have also enabled synthesis of the various metal NPs; this synthetic route has emerged owing to a growing interest in the fundamental physics, chemistry and engineering of light sources (Ma *et al.*, 2000; Rosenberg *et al.*, 1998; Borse *et al.*, 2004*a*,*b*; Yang *et al.*, 2006; Wang *et al.*, 2011; Karadas *et al.*, 2005; Lee *et al.*, 2003; Remita *et al.*, 2005, 2007; Dey, 2005, 2011; Bárta *et al.*, 2010; Yamaguchi *et al.*, 2015, 2016; Bhati *et al.*, 2016). In particular, the advantage of performing radiolysis using synchrotron radiation is its atomic level of processing accuracy; fine control

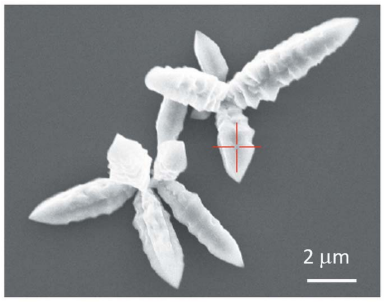

is possible over irradiation parameters such as photon energy, band width, flux, polarization and elapsed time. Recently, Bhati *et al.* (2016) and Yamaguchi *et al.* (2016) have demonstrated that the synthesis of particles can also be performed by monochromatic X-ray irradiation.

The synchrotron radiolysis of metallic NPs has also become a focus in engineering applications because it enables the generation of NPs from aqueous solutions of metal salts. In addition, nanostructures can be tailored by immobilizing NPs at a target location (Ma *et al.*, 2000; Rosenberg *et al.*, 1998; Yamaguchi *et al.*, 2015, 2016). These noble-metal NP nanostructures are typically used for surface-enhanced Raman scattering spectroscopy and plasmon-assisted photochemical reactions (Kreibig & Vollmer, 1995; Le Ru & Etchegoin, 2009; Lu *et al.*, 2009; Cushing *et al.*, 2004; Yamaguchi *et al.*, 2015).

Cupric oxide (Cu_2O, CuO) NPs which are p-type semiconductor materials with a low band gap energy have recently attracted much attention (Zhang *et al.*, 2005, 2006, 2014; Su *et al.*, 2014; Poizot *et al.*, 2000; Volanti *et al.*, 2008; Kim *et al.*, 2010; Park *et al.*, 2012; Debbichi *et al.*, 2012; Long *et al.*, 2009; Dar *et al.*, 2009; Yeh *et al.*, 1999; Radi *et al.*, 2010; Izaki *et al.*, 2007; Fleisch & Mains, 1982; Tamaki *et al.*, 1998; Zaman *et al.*, 2011, 2012; Shao *et al.*, 2007; Clay & Cohen, 1998; Lisiecki & Pileni, 1993; Brookshier *et al.*, 1999). They have been used in the anodes of lithium ion cells, combined with ZnO in heterostructure solar-cell panels (Izaki *et al.*, 2007), and incorporated into gas sensors (Su *et al.*, 2014; Tamaki *et al.*, 1998) and pH sensors (Zaman *et al.*, 2011, 2012). Cupric NPs have favorable characteristics; they are non-toxic, environmentally friendly, highly stable and recyclable. Consequently, many methods have been developed to synthesize and characterize cupric oxide NPs.

In this study, we demonstrate for the first time the synthesis of micrometer- and submicrometer-scale cupric oxide (CuO, Cu_2O) particles using the X-ray synchrotron radiolysis from copper (II) acetate [$Cu(CH_3COO)_2$] solution. The synthesized cupric oxide particles exhibit unique morphologies that resemble caltrops, which are antipersonnel weapons made up of two or more sharp nails or spines; they have traditionally been used to slow the advance of horses, war elephants and human troops. In Japan, ninjas often used caltrops, called 'makibishi', to damage the wheels of vehicles. The particle shape is very interesting and unique. Experimental results show that the morphology and size of cupric oxide particles are strongly dependent on the amount of ethanol in the reaction mixture. The result provides novel knowledge associated with the physical and chemical mechanisms of nucleation and growth of particles in X-ray radiolysis synthesis. Further characterization was performed using microscopic Raman spectroscopy. The synthetic method can be easily controlled to generate highly pure, dispersed cupric oxide particles. This study sheds light on a novel scientific field in which the physics and chemistry of interfacial growth mechanisms can be controlled by the electronic state of the material.

2. Experimental

The stock solution was made by dissolving 6.8 g of $Cu(CH_3COO)_2$ (Wako Chemical, 99.99%) in 100 ml of doubly distilled water. A 100 ml aliquot of 0.37 mol L^{-1} (*M*) $Cu(CH_3COO)_2$ was prepared by diluting the stock solution. We syphoned off 200 µL of the 0.37 *M* $Cu(CH_3COO)_2$ solution into a microtube and added 10 µL of ethanol to obtain the mixed solution. An 18 µL aliquot of the mixed solution was then exposed to X-ray irradiation.

The NPs deposition experiments using synchrotron radiation were performed on BL8S1 at the Aichi Synchrotron Radiation Center (Aichi SRC). The storage ring current and energy were in operation at 300 mA and 1.2 GeV with superbending magnets of 5 T. The X-ray spectra at positions where the flux changes are displayed in Fig. 1. The experimental setup is also shown schematically in Fig. 1, and the platform for the experiment is based on our previous work (Yamaguchi *et al.*, 2015). In this study, the irradiation of white X-rays with beam size of 10 mm × 10 mm was performed. A stainless used steel (SUS) mask on a SiN membrane can form contrast for X-ray irradiation. The use of the X-ray mask allows us to easily obtain about tenfold difference of the photon number in an area directly irradiated by the X-rays with respect to the area covered with the SUS mask. A hole-array consisting of a through-hole of diameter 300 µm was used for this X-ray irradiation experiment. As described in the previous work (Yamaguchi *et al.*, 2015), we introduced the appropriate amount of metallic materials into a precursor solution. A silicon substrate (10 mm × 10 mm × 0.5 mm) was dipped

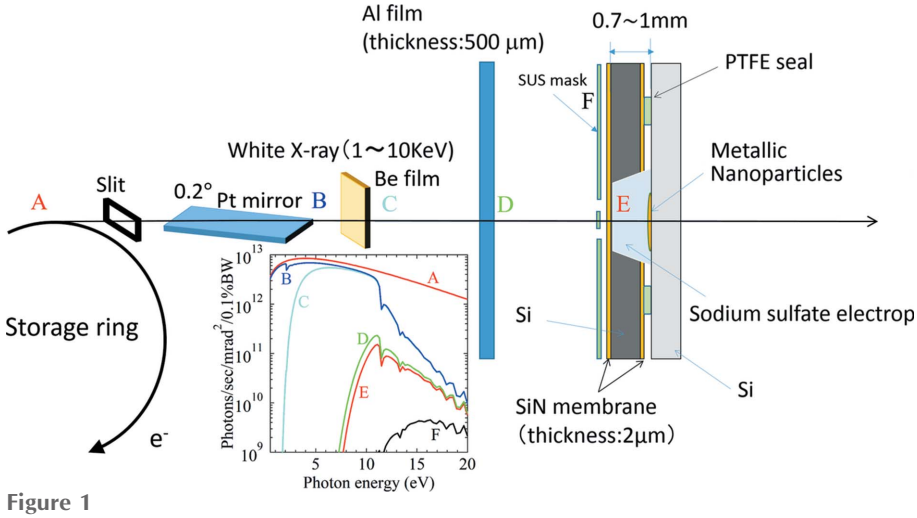

Figure 1
Layout of the X-ray irradiation experiment at BL8S1, Aichi SRC. X-ray spectra are shown in the inset. Photon intensity obtained from (A) synchrotron radiation at BL8S1 of Aichi SRC, (B) Pt mirror (incident angle: 0.2°), (C) 400 µm-thick Be film, (D) 500 µm-thick Al film, (E) metallic solution through air (1 m distance) and (F) 180 µm-thick steel used stainless (SUS) mask.

into the 18 µL solution and the specimen was placed on the irradiation system. The specimen was exposed to 5 min of synchrotron X-rays and then washed using deionized water; this removed residual dross but not the NPs. The NPs on the silicon substrate were examined by field emission scanning electron microscopy (FE-SEM; Jeol JSM-7001F), and energy-dispersive X-ray spectroscopy (EDX) was used to perform elemental analysis. In addition, we obtained Raman spectra using a micro-Raman spectrometer (JASCO; NRS-5100). The excitation source had a wavelength of 532 nm (a green laser), a power of 3.2 mW and was magnified using a 100× field lens. The laser spot diameter was about 1 µm. All experiments were performed at room temperature and in ambient atmosphere.

3. Results and discussion

No NPs were synthesized when silicon substrate was immersed in an aqueous $Cu(CH_3COO)_2$ solution without ethanol and then exposed to X-rays. When ethanol was added to the $Cu(CH_3COO)_2$ solution, X-ray irradiation drove the synthesis of copper particles. Scanning electron microscope (SEM) images of the silicon substrate at different magnifications are shown in Fig. 2. The samples were made from the $Cu(CH_3COO)_2$ solution blended with ethanol in the volumetric ratio 1:20; they received 5 min of X-ray irradiation. The lowest magnification SEM images show several well defined slit patterns [Fig. 2(*a*)]. When magnified, the circular-slit patterns are found to contain nanoparticles, as shown in Fig. 2(*b*). The magnified SEM images of small particles are presented in Figs. 2(*c*)–(*f*). These figures indicate that all the primary particles were caltrop-shaped; no other morphologies were observed. Individual caltrop particles were composed of stacked layers similar to a mille-feuille, as shown in the magnified SEM images. These particles were very stable to solvents, even after washing, and remained on the surface of the substrate, as shown in Fig. 2. The fantastic particle shapes are expected to offer an interesting insight into the nucleation and growth of particles.

Elementary analysis was performed on the synthesized particles using EDX. The red crosshairs in the magnified SEM image (inset of Fig. 3) denote the point analysis position at which EDX was measured. The EDX spectrum in Fig. 3 indicates that the particle is made of copper oxide. A Si peak was neglected because it was a background signal from the substrate. The elemental ratio Cu:O in at% was 72.09:21.44, which corresponded to 3.4 times as many Cu atoms as O atoms. This result suggests that the caltrop particles comprise a mixture of species, such as Cu, CuO, Cu_2O and Cu_4O_3.

We measured the micro-laser Raman scattering spectra in order to determine the composition of the cupric oxide particles. Micro-laser Raman scattering spectra of the Si substrate, a caltrop particle on the Si substrate, a SiN membrane and a caltrop particle on the SiN membrane are illustrated in Figs. 4(*a*)–4(*d*), respectively. The insets in Figs. 4(*b*) and 4(*d*) are optical micrographs that indicate the positions where micro-laser Raman spectra were measured; the bright green spots are the areas that were irradiated by the excitation green laser. Comparing the Raman spectra shown in Figs. 4(*a*) and 4(*b*), a peak at 520 cm^{-1} is deduced to be the Raman signal from the Si substrate because it is not observed

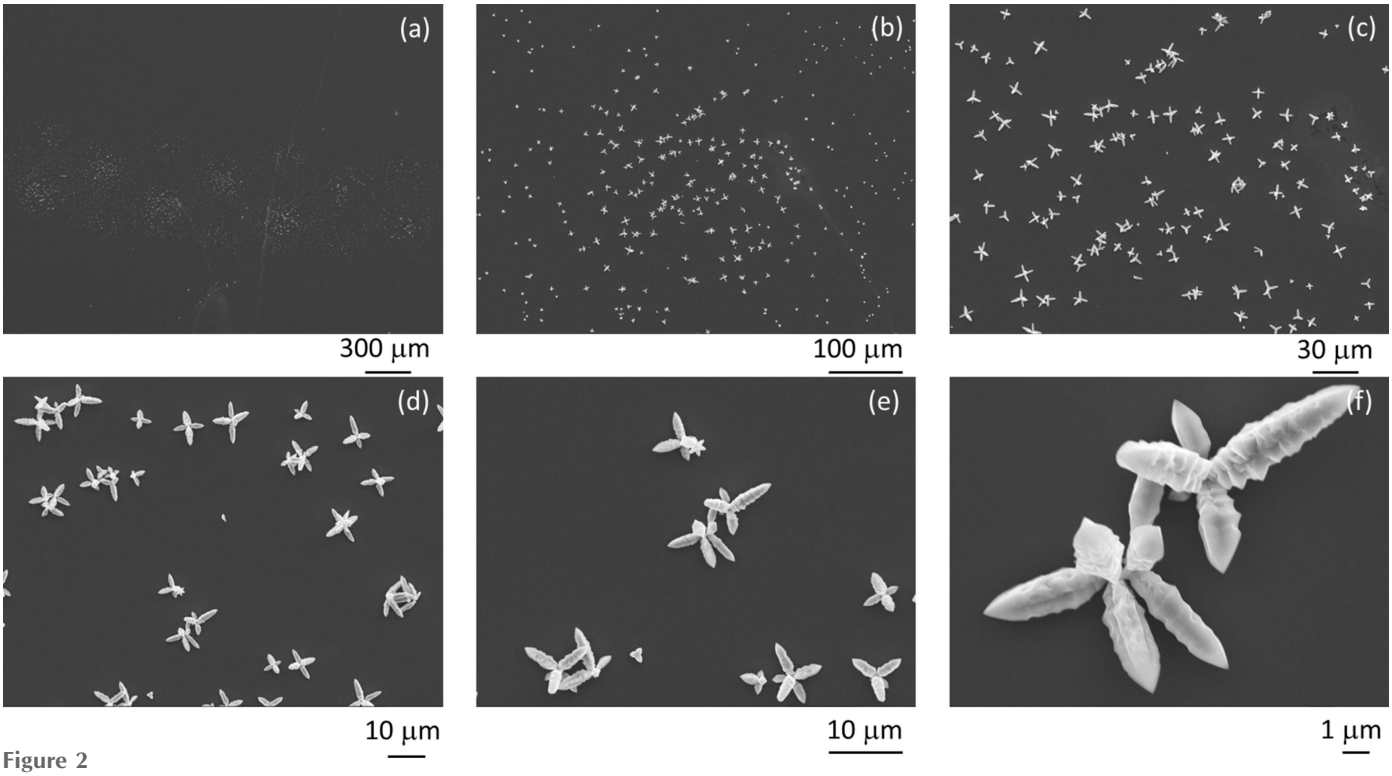

Figure 2
SEM images of silicon substrates dipped in an aqueous $Cu(CH_3COO)_2$ solution spiked with ethanol and irradiated with X-rays from a synchrotron source for 5 min using an X-ray mask. (*a*) The well patterned surface and (*b*)–(*f*) CuO particles.

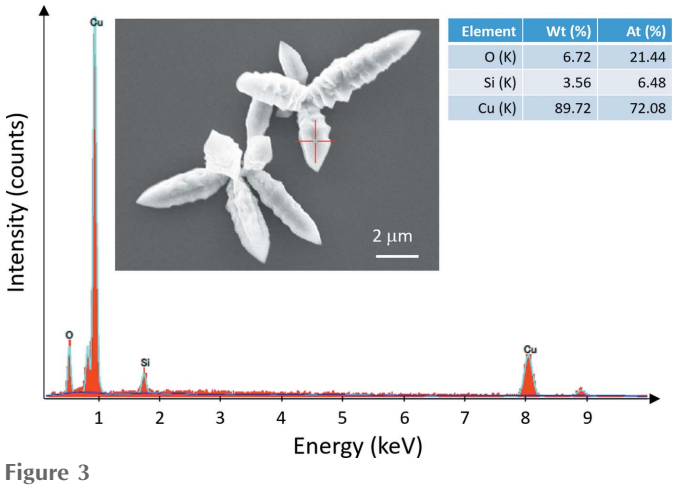

Figure 3
EDX spectrum of cuprous oxide caltrop particles. The inset shows a high-resolution SEM image of the CuO particles. The red crosshairs denote the point analysis position for the EDX measurement.

in Figs. 4(*c*) and 4(*d*), and peaks at 283, 333 and 622 cm^{-1} correspond to Raman signals from Ag (283.8 cm^{-1}) and Bg (333.5 and 622.5 cm^{-1}) modes of cupric oxide CuO, respectively (Zhang *et al.*, 2014; Volanti *et al.*, 2008; Debbichi *et al.*, 2012). The Raman spectrum of cupric oxide was in good agreement with the previous Raman studies (Zhang *et al.*, 2014; Volanti *et al.*, 2008; Debbichi *et al.*, 2012). In the present stage, we found that there are no peaks from other copper oxides, such as Cu_2O and Cu_4O_3. However, the possibility of the existence of other cupric oxide materials included in the synthesized particles is not completely contradicted because the general micro-Raman spectrometer is so sensitive that it can pick up information at a focal depth of about 500 nm. The Raman spectra baselines in Figs. 4(*b*) and 4(*d*) are relatively higher than those in the previous studies (Zhang *et al.*, 2014; Volanti *et al.*, 2008; Debbichi *et al.*, 2012). This indicates that the component originating from Cu contributes to the Raman spectra. The measured Raman spectrum in Fig. 4(*b*) is considered to be superimposed by contributions from Cu, CuO of the synthesized particles and Si substrate, while the spectrum in Fig. 4(*c*) is expected to be derived from Cu and CuO. As a result, this enabled us to determine that the synthesized caltrop particles comprised Cu and CuO by considering the result of the EDX analysis.

In previous studies that have synthesized CuO particles (Zhang *et al.*, 2014; Volanti *et al.*, 2008; Debbichi *et al.*, 2012), CuO plates were mainly oriented on the [001] zone axis and grew prefentially in the [100] and [010] directions. Zaman *et al.* investigated the crystallinity of CuO nanoflowers using X-ray diffraction (Zaman *et al.*, 2011, 2012). They showed that all of the characterization peaks could be assigned to the monoclinic phase of CuO; however, they did not generate caltrop particles. Urchin-like CuO particles, which were more similar to the caltrop particles, were synthesized by several groups. For example, Kim *et al.* (2010) found that the growth direction of the urchin-like CuO particles was very complex; surface facets in the CuO branches were mostly in the [311] direction. This finding was exceptional because {100} and {111} facets would have been lower-energy surfaces. According to Zhang *et al.* (2005), CuO NPs oriented one-dimensionally in the {001} plane during the early stages of aggregation; this is followed by formation of single-crystalline nanostructures comprising hundreds of oriented NPs in a three-dimensionally oriented aggregation of CuO particle. In addition, Su *et al.* (2014) have reported the synthesis of single-crystal copper oxide nanoplatelets with a high percentage of {001} facets using a facile hydrothermal approach. They have reported the surface energies for the relaxed regions of CuO crystal. According to Su *et al.* (2014), the caltrop particles grow along the {010} facet because it is the most stable surface with the lowest energy. The {110} surfaces have the second smallest energy, followed by the {110} surface. The nucleation and growth of caltrop particles with knurled side surfaces is attributed to the flocculation of single-crystal plates that are stacked along the [010] direction. The caltrop CuO particles synthesized in this study are likely to have the same growth mechanism, but this has not been shown decisively. In the near future, we plan to investigate the real-time growth of caltrop CuO particles using X-ray microscopy.

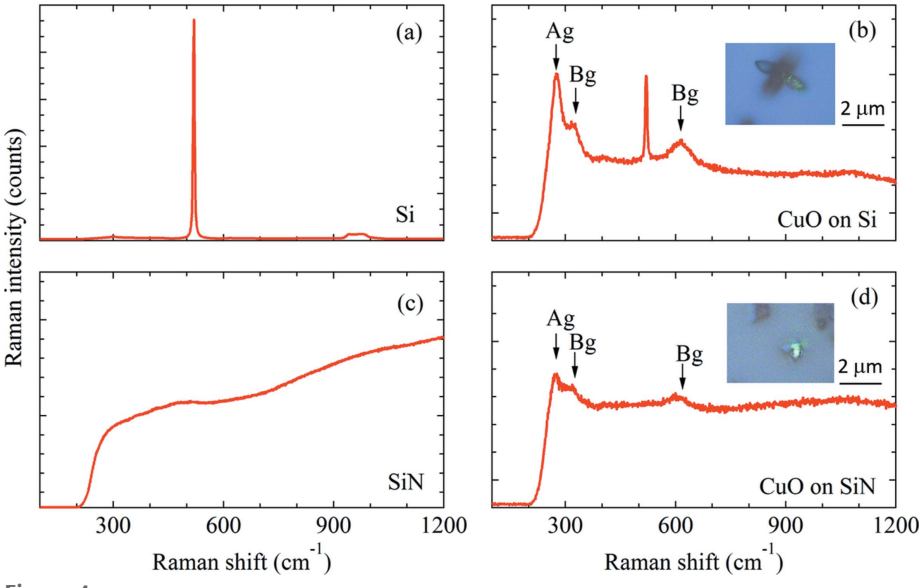

Figure 4
Micro-laser Raman spectra of (*a*) the Si substrate, (*b*) a caltrop CuO particle on the Si substrate, (*c*) the SiN membrane and (*d*) a caltrop CuO particle on the SiN membrane. Optical micrographs inset into (*b*) and (*d*) show the positions of the measurement, indicated by the green light reflected from the excitation laser (wavelength 532 nm). The characteristic Raman modes Ag and Bg are indicated in the spectra of (*b*) and (*d*).

We found that the caltrop particles could also be synthesized on SiN membranes. The particles were smaller than those synthesized on a Si substrate; this is evident from a

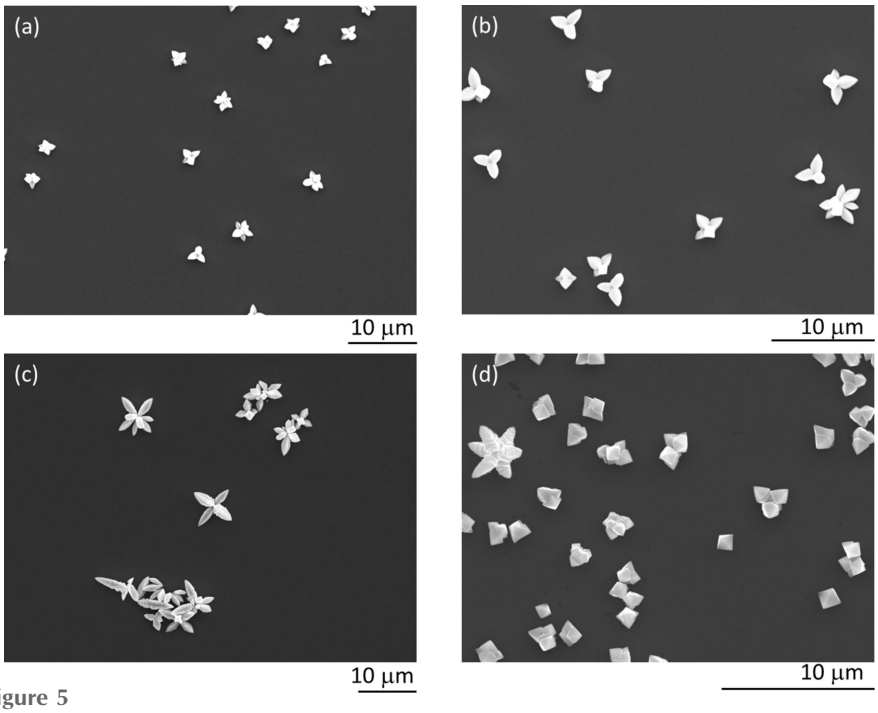

Figure 5
SEM images of CuO particles synthesized by X-ray irradiation using a synchrotron source; different ratios of ethanol to an aqueous $Cu(CH_3COO)_2$ solution were used: (*a*) 3000:1, (*b*) 2000:1, (*c*) 20:1 and (*d*) 2:1. The corresponding ratios described in molar concentration are $Cu(CH_3COO)_2$:ethanol = (*a*) $0.37:5.72 \times 10^{-3}$, (*b*) $0.37:8.17 \times 10^{-3}$, (*c*) $0.37:8.17 \times 10^{-2}$ and (*d*) $0.36\ M:8.17 \times 10^{-1}\ M$.

comparison of the results shown in Figs. 4(*c*) and 4(*d*). Nucleation and growth of the particles appear to occur *via* an electron-donation mechanism during the X-ray irradiation of the Si substrate (Radi *et al.*, 2010). These results indicate that there are several mechanisms for the nucleation and growth of particles. The electron-donation process may be able to accelerate the synthesis of particles.

We varied the amount of ethanol in the initial solution to rigorously investigate its effect on the synthesis of particles. SEM images for samples prepared with varying amounts of ethanol are shown in Fig. 5. The volumetric ratios $Cu(CH_3COO)_2$:ethanol were (*a*) 3000:1, (*b*) 2000:1, (*c*) 20:1 and (*d*) 2:1. The corresponding ratios described in molar concentration are $Cu(CH_3COO)_2$:ethanol = (*a*) $0.37:5.72 \times 10^{-3}$, (*b*) $0.37:8.17 \times 10^{-3}$, (*c*) $0.37:8.17 \times 10^{-2}$ and (*d*) $0.36\ M:8.17 \times 10^{-1}\ M$, respectively. Samples with less ethanol than 3000:1 [$Cu(CH_3COO)_2$:ethanol = $0.37\ M:5.72 \times 10^{-3}\ M$] did not result in the synthesis of particles. Nor were particles generated at ratios greater than 2:1 [$Cu(CH_3COO)_2$:ethanol = $0.36\ M:8.17 \times 10^{-1}\ M$]. That is, the synthesis of particles was only possible for a particular range of ethanol concentrations: from 1/3000 ($5.72 \times 10^{-3}\ M$) to 1/2 ($8.17 \times 10^{-1}\ M$). SEM micrographs revealed that the shape and size of particles was also dependent on the concentration of ethanol. High-resolution SEM images of the particles synthesized with varying amounts of ethanol are presented in Figs. 6(*a*)–6(*d*). The SEM images which are ordered and numbered by the indices (i) and (ii) show some typical particles. As shown in these SEM images, we found that the caltrop particles and Kompetio-like particles (these have a confetti-like shape that resembles sugar candy covered in bulges) were simultaneously synthesized [Figs. 6(*a*)-(i) and 6(*c*)-(ii)]. Octahedral crystals were also generated, as shown in Fig. 6(*d*). According to the previous works (Zhang *et al.*, 2014), Kompeito-like particles grow preferentially in the [100], [010] and [001] directions.

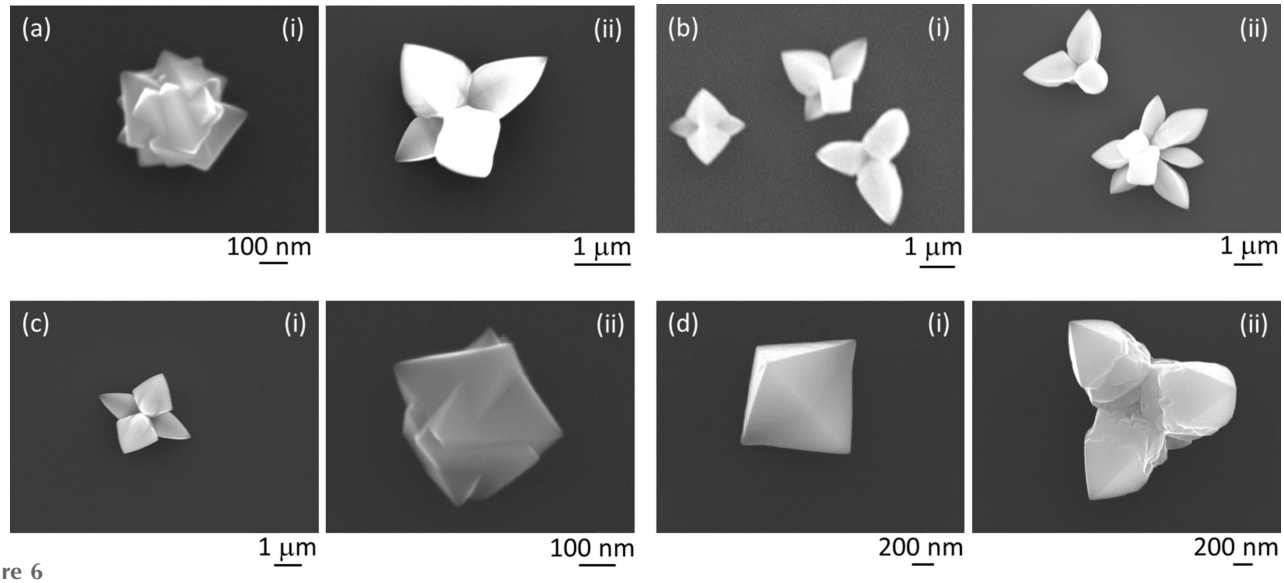

Figure 6
High-resolution SEM images of CuO particles synthesized by synchrotron X-ray radiation of aqueous solutions of $Cu(CH_3COO)_2$ and ethanol in the ratios (*a*) 3000:1, (*b*) 2000:1, (*c*) 20:1 and (*d*) 2:1. Particles observed in different areas are magnified in the SEM images indexed as (i) and (ii).

Both Kompetito-like particles and octahedral crystals are adequately smaller than the caltrop particles, being candidates of nuclei to grow the caltrop particles.

These SEM micrographs were also used to evaluate the average length of petals of the caltrop CuO particles; this length is indicated in the inset of Fig. 7(*c*). The distribution of petal lengths is shown in Fig. 7 for the 60 to 120 petals in each micrograph shown in Figs. 2 and 5. Fig. 7 shows the petal length distribution for samples synthesized from solutions with different volumetric fractions of ethanol. For the cases of the (*a*) smallest and (*e*) largest amounts of ethanol, the average petal length is small, and its distribution is narrow. In contrast, the distribution is broad for intermediate ethanol ratios: 1/2000, 1/200 and 1/20. The dependence of the petal length on the concentration of ethanol is summarized in Fig. 7(*f*). The average size and standard deviation of the petals depended upon the concentration of ethanol, up to the saturation concentration of 1/20. This trend was qualitatively predicted by typical reaction kinetics, whereby the added ethanol shows the reaction by adsorbing onto the surface of particles, preventing their growth.

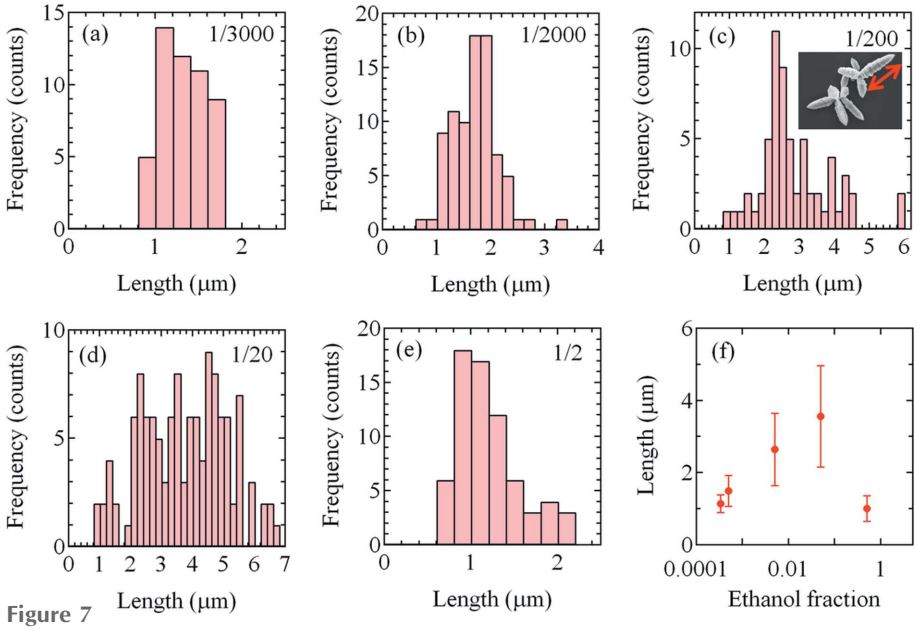

Figure 7
Average distribution of petal lengths for the CuO caltrop particles as measured from ~60–120 petals in each micrograph. The ratio of ethanol to an aqueous solution of $Cu(CH_3COO)_2$ used to synthesize the particles was (*a*) 1/3000, (*b*) 1/2000, (*c*) 1/200, (*d*) 1/20 and (*e*) 1/2. The micrographs used for measurements are shown in Figs. 2 and 5. The petal length is shown in the inset of (*c*). (*f*) The average particle size as a function of the fraction of ethanol.

The micro-Raman spectra of CuO particles synthesized from solutions with various concentrations of ethanol are shown in Fig. 8. Comparing these results with those in Fig. 4(*b*), we find that the Raman spectra are independent of the amount of ethanol. This result indicates that the composition of particles was nearly identical between samples despite having been synthesized from different concentrations of ethanol. The size of the particles was dependent on the concentration of ethanol but their composition was not.

When aqueous solutions absorb ionizing radiation, the X-rays cause radiolysis of the water and create reactive radicals and radical ions according to the following reaction (Ma *et al.*, 2000; Rosenberg *et al.*, 1998; Borse *et al.*, 2004*a*,*b*; Yang *et al.*, 2006; Wang *et al.*, 2011; Karadas *et al.*, 2005; Lee *et al.*, 2003; Remita *et al.*, 2005, 2007; Dey, 2011; Bárta *et al.*, 2010; Yamaguchi *et al.*, 2015, 2016; Bhati *et al.*, 2016; Weiss, 1944, 1946; Miller, 1950; Samuel & Magee, 1953; Johnsen *et al.*, 1969; Buxton *et al.*, 1988),

$$H_2O \xrightarrow{\text{X-ray radiation}} e^-_{aq},\ H_3O^+,\ H\cdot,\ OH\cdot \qquad (1)$$

The main reducing species are solvated electrons (e^-_{aq}) and hydrogen radicals (H·). The OH· radical is a strong oxidant; therefore, it is necessary to introduce an OH· scavenger into the aqueous solution to enable reduction of the metallic ions,

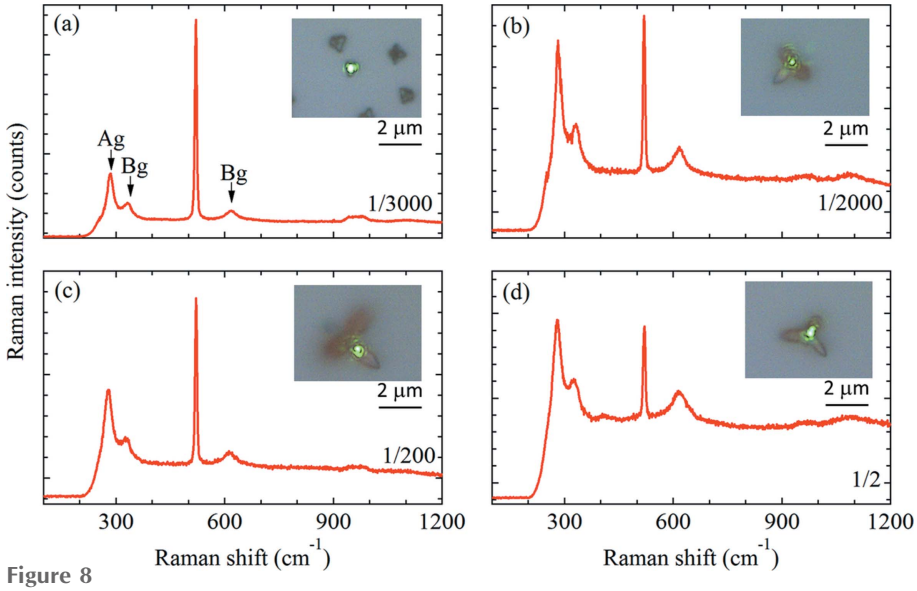

Figure 8
Micro-laser Raman spectra of CuO particles synthesized by the X-ray irradiation of aqueous $Cu(CH_3COO)_2$ solution with different volumetric ratios of ethanol: (*a*) 3000:1, (*b*) 2000:1, (*c*) 200:1 and (*d*) 2:1. The corresponding ratios described in molar concentration are $Cu(CH_3COO)_2$:ethanol = (*a*) $0.37:5.72 \times 10^{-3}$, (*b*) $0.37:8.17 \times 10^{-3}$, (*c*) $0.37:8.17 \times 10^{-2}$ and (*d*) $0.36\ M:8.17 \times 10^{-1}\ M$. The insets are optical micrographs of the particles; the position of the green light indicates the measurement position of the excitation laser (wavelength 532 nm).

which is essential for the nucleation and growth of particles. Additional species are generated from the radiation of ethanol and coordinated water molecules in the $Cu(CH_3COO)_2$ solution, as shown below (Ma *et al.*, 2000; Rosenberg *et al.*, 1998; Borse *et al.*, 2004*a*,*b*; Yang *et al.*, 2006; Wang *et al.*, 2011; Karadas *et al.*, 2005; Lee *et al.*, 2003; Remita *et al.*, 2005, 2007; Dey, 2011; Bárta *et al.*, 2010; Yamaguchi *et al.*, 2015, 2016; Bhati *et al.*, 2016; Weiss, 1944, 1946; Miller, 1950; Samuel & Magee, 1953; Johnsen *et al.*, 1969; Buxton *et al.*, 1988),

$$CH_3CH_2OH \longrightarrow e^-_{aq}, CH_3CH_2OH^+ \quad (2)$$

$$e^-_{aq} + OH\cdot \longrightarrow OH^- \quad (3)$$

These anions and cations are the precursors to CuO. As a result, the following reaction can be induced:

$$Cu(CH_3COO)_2 + H_2O \overset{\text{X-ray \& } CH_3CH_2OH}{\longrightarrow} CuO + 2CH_3COOH$$

X-ray irradiation of the $Cu(CH_3COO)_2$ solution in the presence of ethanol results in caltrop CuO particles through the nucleation process shown in Figs. 2, 5 and 6. The petal size distribution shown in Fig. 7 indicates that the nucleation and growth process can be explained by the LaMer model (LaMer & Dinegar, 1950). Comparison of the particle sizes on the Si substrate and SiN membrane (shown in Fig. 3) indicates that the H-terminated Si substrate plays an important role in the synthesis of particles, as described by Radi *et al.* (2010). Notably, there is no direct evidence to support the proposed synthetic and chemical routes; the true mechanism may be more sophisticated. The nucleation and growth of caltrop CuO particles have not been reported as yet; the process using synchrotron radiation X-ray irradiation enables these caltrop CuO particles to nucleate and grow directly from $Cu(CH_3COO)_2$ solution at the lowest temperature (ambient temperature) and duration time (below 1 s without Al plate to attenuate X-rays), compared with the previous studies (Zhang *et al.*, 2005, 2006, 2014; Su *et al.*, 2014; Poizot *et al.*, 2000; Volanti *et al.*, 2008; Kim *et al.*, 2010; Park *et al.*, 2012; Debbichi *et al.*, 2012; Long *et al.*, 2009; Dar *et al.*, 2009; Yeh *et al.*, 1999; Radi *et al.*, 2010; Izaki *et al.*, 2007; Fleisch & Mains, 1982; Tamaki *et al.*, 1998; Zaman *et al.*, 2011, 2012; Shao *et al.*, 2007; Clay & Cohen, 1998; Lisiecki & Pileni, 1993; Brookshier *et al.*, 1999).

Based on high-resolution SEM images, EDX mapping and micro-Raman spectroscopy, we demonstrated the synthesis of the caltrop particles including CuO from aqueous solutions exposed to X-ray irradiation. The facile process of irradiating solutions with X-rays enables the synthesis of nanoscale and micrometer-scale particles for fundamental investigations and applications, such as drug delivery, solar systems, catalysis, printed circuits and novel lithographite galvanoformung abformung (LIGA) processes (Saile *et al.*, 2009). Caltrop CuO particles are a promising candidate for the absorption of CO and CO_2; they also have potential applications in solar cells and sensors as well as catalysts to combat global warming (Su *et al.*, 2014; Moreno *et al.*, 2015; Pal *et al.*, 2014).

4. Conclusion

The present work demonstrates that CuO NPs can be obtained *via* a one-step synthesis in which an aqueous $Cu(CH_3COO)_2$ solution mixed with ethanol is exposed to X-ray irradiation at a synchrotron source. The synthesized caltrop NPs form higher-order nanostructures. Using high-resolution SEM microscopy and micro-Raman spectroscopy, we determine that the caltrop NPs comprise Cu and CuO. The alcohol that is added to the stick solution enables the copper ions to reduce the caltrop particles. Two potential challenges have been identified: (i) the synthesis process, *i.e.* the nucleation and formation of NPs from a liquid solution in the presence of X-ray irradiation with/without alcohol is not fully understood, and (ii) caltrop particles may coagulate. These issues are worthy of further investigation.

Direct X-ray irradiation using a synchrotron radiation source can provide an alternative route for exploring the novel physical mechanisms of liquid/solid interfacial reactions processed in the liquid phase. Higher-order nanostructures consisting of metallic NPs and metal oxide NPs provide an ideal platform to directly induce catalysis and probe which can induce surface-enhanced Raman scattering. This one-step, direct deposition process can be used in new devices such as 'Lab-on-a-chip' and 'μTAS: micron-total-analysis-systems' for chemical and environmental analyses. Although further refinement is needed, the results demonstrated herein show that the room-temperature radiolysis route is a viable technique for synthesizing and constructing higher-order nano-/micro-structures for use in catalysis and sensor technologies. The success of the synthesis and deposition of caltrop including CuO particles will open new doors for developing novel electronics and 'Lab-on-a-chip'.

Acknowledgements

We are grateful to Dr Yamaguchi of Hyogo Prefectural Institute of Technology for SEM and EDX measurement support. We appreciate Dr Saiki and Dr Takizawa of Hyogo Prefectural Institute of Technology for fruitful discussions. This work is partly supported by the Strategic Information and Communications R&D Promotion Programme. These experiments were conducted at BL8S1 of Aichi Synchrotron Radiation Center, Aichi Science and Technology Foundation, Aichi, Japan.

References

Akamatsu, K., Ikeda, S., Nawafune, H. & Yanagimoto, H. (2004). *J. Am. Chem. Soc.* **126**, 10822–10823.
Athawale, A. A., Katre, P. P., Kumar, M. & Majumdar, M. B. (2005). *Mater. Chem. Phys.* **91**, 507–512.
Bae, C. H., Nam, S. H. & Park, S. M. (2002). *Appl. Surf. Sci.* **197–198**, 628–634.
Bárta, J., Pospíšil, M. & Čuba, V. (2010). *J. Radioanal. Nucl. Chem.* **286**, 611–618.
Bhati, A., Bharwaj, R., Agrawal, A. K., Goyal, N. & Gautam, S. (2016). *Sci. Rep.* **6**, 22394.
Borse, P. H., Yi, J. M., Je, J. H., Choi, S. D., Hwu, Y., Ruterana, P. & Nouet, G. (2004*a*). *Nanotechnology*, **15**, S389–S392.

Borse, P. H., Yi, J. M., Je, J. H., Tsai, W. L. & Hwu, Y. (2004*b*). *J. Appl. Phys.* **95**, 1166–1170.
Brookshier, M. A., Chusuei, C. C. & Goodman, D. W. (1999). *Langmuir*, **15**, 2043–2046.
Buxton, G. V., Greenstock, C. L., Helman, W. P. & Ross, A. B. (1988). *J. Phys. Chem. Ref. Data*, **17**, 513–886.
Clay, T. & Cohen, R. E. (1998). *New J. Chem.* **22**, 745–748.
Cushing, A. L., Kolesnichenko, V. L. & O'Connor, C. J. (2004). *Chem. Rev.* **104**, 3893–3946.
Dar, M. A., Ahsanulhaq, Q., Kim, Y. S., Sohn, J. M., Kim, W. B. & Shin, H. S. (2009). *Appl. Surf. Sci.* **255**, 6279–6284.
Debbichi, L., Marco de Lucas, M. C., Pierson, J. F. & Krüger, P. (2012). *J. Phys. Chem. C*, **116**, 10232–10237.
Dey, G. R. (2005). *Radiat. Phys. Chem.* **74**, 172–184.
Dey, G. R. (2011). *Radiat. Phys. Chem.* **80**, 1216–1221.
Fievet, F., Lagier, J., Blin, B., Beaudoin, B. & Figlarz, M. (1989). *Solid State Ionics*, **32–33**, 198–205.
Figlarz, M., Fievet, F. & Lagier, J. P. (1985). French Patent 8 221 483.
Fleisch, T. H. & Mains, G. J. (1982). *Appl. Surf. Sci.* **10**, 51–62.
Frens, G. (1972). *Colloid Polym. Sci.* **250**, 736–741.
Frens, G. (1973). *Nature (London)*, **241**, 20–22.
Gedanken, A. (2004). *Ultrason. Sonochem.* **11**, 47–55.
Hara, R., Fukuoka, T., Takahashi, R., Utsumi, Y. & Yamaguchi, A. (2015). *RSC Adv.* **5**, 1378–1384.
Hashimoto, S., Uwada, T., Hagiri, M. & Shiraishi, R. (2011). *J. Phys. Chem. C*, **115**, 4986–4993.
Izaki, M., Shinagawa, T., Mizuno, K., Ida, Y., Inaba, M. & Tasaka, A. (2007). *J. Phys. D*, **40**, 3326–3329.
Johnsen, R. H., Barker, N. T. & Burgin, M. (1969). *J. Phys. Chem.* **73**, 3204–3208.
Karadas, F., Ertas, G., Ozkaraoglu, E. & Suzer, S. (2005). *Langmuir*, **21**, 437–442.
Kim, J. Y., Park, J. C., Kang, H., Song, H. & Park, H. (2010). *Chem. Commun.* **46**, 439–441.
Kreibig, U. & Vollmer, M. (1995). *Optical Properties of Metal Clusters, Springer Series in Material Science*, Vol. 25. Berlin: Springer.
Kurihara, L. K., Chow, G. M. & Schoen, P. E. (1995). *Nanostruct. Mater.* **5**, 607–613.
Kvítek, L., Panáček, A., Soukupová, J., Kolář, M., Večeřová, R., Prucek, R., Holecová, M. & Zbořil, R. (2008). *J. Phys. Chem. C*, **112**, 5825–5834.
LaMer, V. K. & Dinegar, R. H. (1950). *J. Am. Chem. Soc.* **72**, 4847–4854.
Lee, H. J., Je, J. H., Hwu, Y. & Tsai, W. L. (2003). *Nucl. Instrum. Methods Phys. Res. B*, **199**, 342–347.
Le Ru, E. C. & Etchegoin, P. G. (2009). *Principles of Surface-Enhanced Raman Spectroscopy and Related Plasmonic Effects.* Amsterdam: Elsevier.
Lisiecki, I. & Pileni, M. P. (1993). *J. Am. Chem. Soc.* **115**, 3887–3896.
Long, J., Dong, J., Wang, X., Ding, Z., Zhang, Z., Wu, L., Li, Z. & Fu, X. (2009). *J. Colloid Interface Sci.* **333**, 791–799.
Lu, X., Rycenga, M., Skrabalak, S. E., Wiley, B. & Xia, Y. (2009). *Annu. Rev. Phys. Chem.* **60**, 167–192.
Ma, Q., Moldovan, N., Mancini, D. C. & Rosenberg, R. A. (2000). *Appl. Phys. Lett.* **76**, 2014–2016.
Mafuné, F., Kohno, J., Takeda, Y. & Kondow, T. (2003). *J. Phys. Chem. B*, **107**, 4218–4223.
Miller, N. (1950). *J. Chem. Phys.* **18**, 79–87.
Moreno, J. L. V., Arevalo, R. L., Escaño, M. C. S., Padama, A. A. B. & Kasai, H. (2015). *J. Phys. Soc. Jpn*, **84**, 015003.
Nagata, Y., Watananabe, Y., Fujita, S., Dohmaru, T. & Taniguchi, S. (1992). *J. Chem. Soc. Chem. Commun.* **21**, 1620–1622.
Okitsu, K., Yue, A., Tanabe, S., Matsumoto, H. & Yobiko, Y. (2001). *Langmuir*, **17**, 7717–7720.
Pal, J., Ganguly, M., Dutta, S., Mondal, C., Negishi, Y. & Pal, T. (2014). *CrystEngComm*, **16**, 883–893.
Park, J. C., Kim, A. Y., Kim, J. Y., Park, S., Park, K. H. & Song, H. (2012). *Chem. Commun.* **48**, 8484–8486.
Poizot, P., Laruelle, S., Grugeon, S., Dupont, L. & Tarascon, J. M. (2000). *Nature (London)*, **407**, 496–499.
Radi, A., Pradhan, D., Sohn, Y. & Leung, K. T. (2010). *ACS Nano*, **4**, 1553–1560.
Remita, S., Fontaine, P., Lacaze, E., Borensztein, Y., Sellame, H., Farha, R., Rochas, C. & Goldmann, M. (2007). *Nucl. Instrum. Methods Phys. Res. B*, **263**, 436–440.
Remita, S., Fontaine, P., Rochas, C., Muller, F. & Goldmann, M. (2005). *Eur. Phys. J. D*, **34**, 231–233.
Rosenberg, R. A., Ma, Q., Lai, B. & Macini, D. C. (1998). *J. Vac. Sci. Technol. B*, **16**, 3535.
Saile, V., Wallradbe, U., Tabata, O. & Korvink, J. G. (2009). *Advanced Micro and Nanosystems*, Vol. 7, *LIGA and its Applications.* Weinheim: Wiley.
Samuel, A. H. & Magee, J. L. (1953). *J. Chem. Phys.* **21**, 1080–1087.
Shao, W., Pattanaik, G. & Zangari, G. (2007). *J. Electrochem. Soc.* **154**, D339–D345.
Su, D., Xie, X., Dou, S. & Wang, G. (2014). *Sci. Rep.* **4**, 5753.
Suslick, K. S., Choe, S., Cichowlas, A. A. & Grinstaff, M. W. (1991). *Nature (London)*, **353**, 414–416.
Takami, A., Kurita, H. & Koda, S. (1999). *J. Phys. Chem. B*, **103**, 1226–1232.
Tamaki, J., Shimanoe, K., Yamada, Y., Yamamoto, Y., Miura, N. & Yamazoe, N. (1998). *Sens. Actuators B*, **49**, 121–125.
Tsuji, M., Hashimoto, M., Nishizawa, Y., Kubokawa, M. & Tsuji, T. (2005). *Chem. Eur. J.* **11**, 440–452.
Tu, W. & Liu, H. (2000). *J. Mater. Chem.* **10**, 2207–2211.
Volanti, D. P., Keyson, D., Cavalcante, L. S., Simões, A. Z., Joya, M. R., Longo, E., Varela, J. A., Pizani, P. S. & Souza, A. G. (2008). *J. Alloys Compd.* **459**, 537–542.
Wagner, J., Kirner, T., Mayer, G., Albert, J. & Köhler, J. M. (2004). *Chem. Eng. J.* **101**, 251–260.
Wagner, J. & Köhler, M. (2005). *Nano Lett.* **5**, 685–691.
Wang, B.-L., Hsao, B. J., Lai, S. F., Chen, W. C., Chen, H. H., Chen, Y. Y., Chien, C. C., Cai, X., Kempson, I. M., Hwu, Y. & Margaritondo, G. (2011). *Nanotechnology*, **22**, 065605.
Wiley, B., Herricks, T., Sun, Y. & Xia, Y. (2004). *Nano Lett.* **4**, 1733–1739.
Yamaguchi, A., Matsumoto, T., Okada, I., Sakurai, I. & Utsumi, Y. (2015). *Mater. Chem. Phys.* **160**, 205–211.
Yamaguchi, A., Okada, I., Fukuoka, T., Sakurai, I. & Utsumi, Y. (2016). *Jpn. J. Appl. Phys.* **55**, 055502.
Yamamoto, T., Wada, Y., Sakata, T., Mori, H., Goto, M., Hibino, S. & Yanagida, S. (2004). *Chem. Lett.* **33**, 158–159.
Yang, Y.-C., Wang, C., Hwu, Y. & Je, J. (2006). *Mater. Chem. Phys.* **100**, 72–76.
Yeh, M.-S., Yang, Y., Lee, Y., Lee, H., Yeh, Y. & Yeh, C. (1999). *J. Phys. Chem. B*, **103**, 6851–6857.
Yeung, S., Hobson, R., Biggs, S. & Grieser, F. (1993). *J. Chem. Soc. Chem. Commun.* **4**, 378–379.
Weiss, J. (1944). *Nature (London)*, **153**, 748.
Weiss, J. (1946). *Nature (London)*, **157**, 584.
Zaman, S., Asif, M. H., Zainelabdin, A., Amin, G., Nur, O. & Willander, M. (2011). *J. Electroanal. Chem.* **662**, 421–425.
Zaman, S., Zainelabdin, A., Amin, G., Nur, O. & Willander, M. (2012). *J. Phys. Chem. Solids*, **73**, 1320–1325.
Zhang, J., Liu, J., Peng, Q., Wang, X. & Li, Y. (2006). *Chem. Mater.* **18**, 867–871.
Zhang, Q., Zhang, K., Xu, D., Yang, G., Huang, H., Nie, F., Liu, C. & Yang, S. (2014). *Prog. Mater. Sci.* **60**, 208–337.
Zhang, Z., Sun, H., Shao, X., Li, D., Yu, H. & Han, M. (2005). *Adv. Mater.* **17**, 42–47.